Wave scattering by infinite cylindrical shell structures submerged in a fluid medium

L. Godinho, A. Tadeu*, F.J. Branco

Department of Civil Engineering, University of Coimbra, Polo II—Pinhal de Marrocos, 3030-290 Coimbra, Portugal

Abstract

This work analyzes the wave scattering by an elastic, fluid-filled, cylindrical shell structure submerged in a fluid medium and subjected to the effect of a point pressure load placed inside or outside the cylindrical shell. The shell structures modeled have constant cross-sections along their axis, corresponding to 2.5D problems. A Fourier transformation in the direction in which the geometry does not vary is applied to find the 3D field as the summation of the 2D solutions for different spatial wavenumbers.

The wave propagation patterns are analyzed for shell structures defined by two concentric or non-concentric cylindrical circular surfaces. The boundary element method, formulated in the frequency domain, is used to calculate the dynamic response of these systems when the shell is defined by non-concentric cylindrical circular surfaces, while analytical solutions are used to compute the response when two concentric cylindrical circular surfaces define the shell structure. Different simulations are performed for receivers placed at distinct positions, in order to study the normal modes excited at each load position within each shell structure type. Both frequency and time solutions are obtained, in an attempt to obtain wave propagation features that may be used as a basis for developing non-destructive testing techniques.
© 2003 Elsevier Science B.V. All rights reserved.

1. Introduction

Wave propagation and vibration phenomena have interested researchers for many years. The particular case of the vibration of thin or thick shell structures has been analyzed using many different approaches, ranging from analytical to numerical methods. The latter are applicable to a wide range of situations, and allow the analysis of physical systems with different configurations.

The propagation of guided transient waves in the circumferential direction of annular structural components was addressed by Liu and Qu [1]. Their work used the eigenfunction expansion method to analyze a circular annulus with null traction at the inner surface and subject to a time dependent transient excitation with different incidence angles at the outer surface. This method allowed the contributions of the different eigenmodes to be separated, making it possible to identify the ones making more important contributions to the response. Chung and Lee [2] proposed a new conical ring element to be used in connection with the finite element method to analyze the free

---

* Corresponding author. Tel.: +351-239-797-204; fax: +351-239-797-190.
E-mail address: tadeu@dec.uc.pt (A. Tadeu).

vibrations of nearly axisymmetric shell structures. The element proposed allowed the effect of a possible slight local deviation from the pure axisymmetric form to be taken into account.

The free vibration of rings with profile variations in the circumferential direction was studied by Hwang et al. [3]. Their methodology was based on expressing the inner and the outer profiles as Fourier series, using an iterative numerical procedure to determine the middle surface and thickness at each cross-section. Novozhilov's thin shell theory is then used to model the deformation mechanics of the ring, and eigenfrequencies are determined by the Rayleigh–Ritz method, together with a harmonic series description of the displacements. Several cases were analyzed by Fox et al. [4] using this method, in which the inner and outer profiles are nominally circular with various superimposed harmonic variations in radius. The most important causes of frequency splitting were identified and highlighted. Later, the same method was used [5] to assess the vibration of elliptical rings with a constant or variable cross-section, examining the effect of the aspect ratio of the ellipse and the influence of single harmonic perturbations of the ring profile on the frequency splitting of vibration modes. These results compared well with previously published results for aspect ratios close to unity. However, for aspect ratios significantly different from unity, the additional terms used by the authors increased the accuracy.

When a fluid medium is present inside or outside the structure, more elaborate models that take into account the coupling between the solid and the fluid should be used. Researchers proposed different models to solve problems of this type. The wave scattering by submerged elastic circular cylindrical shells, filled with air, struck by plane harmonic acoustic waves was analyzed by Veksler et al. [6]. They used the standard resonance scattering theory to study the modal resonances, focusing their investigation on the generation of bending waves. They concluded that these waves could be generated when the relative thickness of the shell is not too great, and that the dispersion curves of their phase velocity were limited by the dispersion curves of the free bending modes, when the density of the host fluid tends towards zero.

Bao et al. [7] addressed the existence of various types of circumferential waves and the repulsion of their dispersion curves for the case of a submerged thin elastic circular fluid-filled cylindrical shell. Their study was based on an analytical calculation of the partial-wave resonances in the acoustic scattering amplitude of a normally incident plane wave.

Recent work by Maze et al. [8] presented a study on the various guided acoustic circumferential modes found in a water-filled tube. This work showed, both theoretically and experimentally, that structure waves are present inside a water-filled thin walled tube in vacuum. The group velocities for the first two coupled modes calculated by the authors were in excellent agreement with experimental results.

In many cases, the shell structure may not be perfectly circular, and the interior and exterior surfaces may be defined by two non-concentric circumferences. This deviation from a pure circular form, with constant thickness, introduces variations in the dynamic behavior of the structure. In the present paper, the authors analyze the 3D wave propagation in the vicinity of a fluid-filled cylindrical shell structure, submerged in a continuous homogeneous fluid medium. The full coupling between the external fluid, the elastic material and the internal fluid is taken into account. Two cross-sections are studied, corresponding to shells defined by two concentric or non-concentric circumferences. In both cases, the shell is assumed to be made of a homogeneous elastic material.

A 2.5D formulation was used, taking into account the full 3D nature of the problem. This formulation allowed the authors to obtain 3D responses in the frequency domain as a discrete summation of the 2D solutions for different axial wavenumbers [9]. Analytical solutions are used to solve each of the 2D problems when the thickness of the shell wall is constant, and the boundary element method (BEM) is applied to obtain the response when the cylindrical shell is not perfect. Pressure variations in the fluid medium that fills the shell and the dependence of the different normal modes on the position of the source and geometry of the cross-section are analyzed. A better understanding of the behavior of the dynamic system is gained from the time domain responses, which are obtained using inverse Fourier transforms.

First, this work describes the 2.5D formulation of the scattering problem, the analytical and the BEM frequency solutions. Then, the BEM solution is validated against the analytical solution. Next, the process used to compute time domain results is described. Finally, a set of numerical applications is presented, showing how an infinite
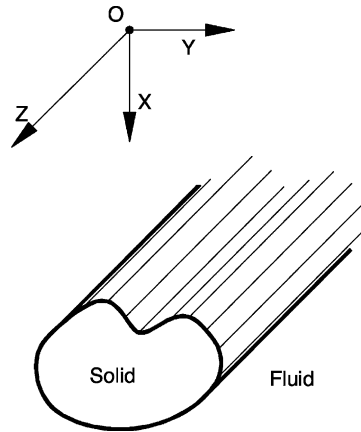
Fig. 1. Geometry of the problem.

cylindrical shell behaves when subjected to the effect of a point source, placed at different positions in the vicinity of shell structures defined by two concentric or non-concentric circumferences.

2. 3D problem formulation

Consider an infinite, fluid-filled, shell structure with cylindrical geometry, as in Fig. 1, submerged in a spatially uniform fluid medium, aligned along the z-axis, and subjected to a harmonic dilatational point source, placed in the exterior fluid medium, oscillating with a frequency ω. The incident field can be expressed by means of the dilatational potential ϕ:

$$\phi_{\text{inc}} = \frac{A\,e^{i(\omega/\alpha_1)\left(\alpha_1 t - \sqrt{(x-x_0)^2 + y^2 + z^2}\right)}}{\sqrt{(x-x_0)^2 + y^2 + z^2}}, \tag{1}$$

where the subscript 'inc' denotes the incident field, A the wave amplitude, α_1 the pressure wave velocity allowed in the exterior fluid medium, $(x_0, 0, 0)$ defines the position of the source and $i = \sqrt{-1}$.

The geometry of this problem remains constant along the z-direction, which allows the incident field to be expressed as a summation of 2D sources, with different spatial wavenumbers, by applying a Fourier transformation along the z-direction:

$$\phi_{\text{inc}}(\omega, x, y, z) = \frac{2\pi}{L} \sum_{m=-\infty}^{\infty} \hat{\phi}_{\text{inc}}(\omega, x, y, k_{zm}) \tag{2}$$

with $\hat{\phi}_{\text{inc}}(\omega, x, y, k_{zm}) = (-iA/2)H_0^{(2)}(k_{\alpha1}((x-x_0)^2 + y^2)^{1/2})\,e^{-ik_{zm}z}$, k_{zm} being the axial wavenumber given by $k_{zm} = (2\pi/L)m$, $k_{\alpha1} = ((\omega^2/\alpha_1^2) - k_{zm}^2)^{1/2}$ (Im $k_{\alpha1} < 0$), $H_n^{(2)}(\cdots)$ the second Hankel functions of order n, and L the distance between virtual point sources equally spaced along z. The distance L must be sufficiently large to avoid spatial contamination from the virtual sources [10].

3. Analytical solution

Consider a circular shell solid structure, defined by the internal and external radii r_A and r_B, respectively, and submerged in a homogenous fluid medium, as illustrated in Fig. 2. A harmonic dilatational source placed in the
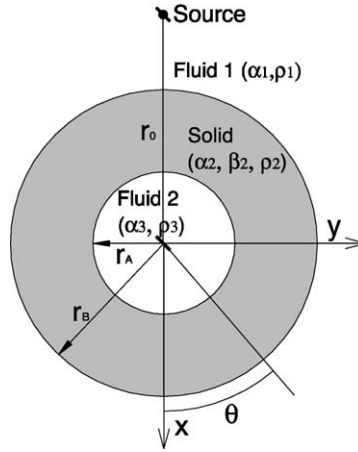
Fig. 2. Circular cylindrical shell structure submerged in a fluid medium.

exterior fluid medium is assumed to illuminate the system, generating waves that hit the surface of the submerged structure. Part of the incident energy is then reflected back to the exterior fluid medium, with the rest being transmitted into the solid material, as propagating body and guided waves. These waves continue to propagate and may eventually hit the inner surface of the structure, where similar phenomena occur.

The wavefield generated in the exterior fluid medium (fluid 1) depends both on the incident pressure waves and those coming from the external surface of the shell. The latter propagate away from the cylindrical shell, and can be defined using the following displacement potential when a cylindrical coordinate system is centered on the axis of the circular shell:

$$\hat{\phi}_1 = \sum_{n=0}^{\infty} A_n^1 H_n(k_{\alpha 1} r) \cos(n\theta) \, e^{-ik_{zm}z}. \tag{3}$$

Inside the solid material of the shell, two distinct groups of waves exist, corresponding to inward travelling waves, generated at the external surface, and outward travelling waves, generated at the internal surface of the shell. Each of these groups of waves can be represented using one dilatational and two shear potentials:

$$\hat{\phi}_2 = \sum_{n=0}^{\infty} A_n^2 J_n(k_{\alpha 2} r) \cos(n\theta) \, e^{-ik_{zm}z}, \qquad \hat{\psi}_2 = \sum_{n=0}^{\infty} A_n^3 J_n(k_{\beta 2} r) \sin(n\theta) \, e^{-ik_{zm}z},$$

$$\hat{\chi}_2 = \sum_{n=0}^{\infty} A_n^4 J_n(k_{\beta 2} r) \cos(n\theta) \, e^{-ik_{zm}z}, \qquad \hat{\phi}_3 = \sum_{n=0}^{\infty} A_n^5 H_n(k_{\alpha 2} r) \cos(n\theta) \, e^{-ik_{zm}z},$$

$$\hat{\psi}_3 = \sum_{n=0}^{\infty} A_n^6 H_n(k_{\beta 2} r) \sin(n\theta) \, e^{-ik_{zm}z}, \qquad \hat{\chi}_3 = \sum_{n=0}^{\infty} A_n^7 H_n(k_{\beta 2} r) \cos(n\theta) \, e^{-ik_{zm}z}, \tag{4}$$

where $k_{\alpha 2} = ((\omega^2/\alpha_2^2) - k_z^2)^{1/2}$, $k_{\beta 2} = ((\omega^2/\beta_2^2) - k_z^2)^{1/2}$ and α_2 and β_2 are, respectively, the dilatational and shear wave velocities permitted in the solid formation.

In the fluid that fills the shell structure (fluid 2), only inward propagating waves are generated. For this case, the relevant dilatational potential is given by

$$\hat{\phi}_4 = \sum_{n=0}^{\infty} A_n^8 J_n(k_{\alpha 3} r) \cos(n\theta) \, e^{-ik_{zm}z}, \tag{5}$$

where $k_{\alpha 3} = ((\omega^2/\alpha_3^2) - k_z^2)^{1/2}$ and α_3 is the pressure wave velocity in the inner fluid. The terms $A_n^j (j = 1, 8)$ for each potential of the expressions (3)–(5) are unknown coefficients to be determined by imposing the required boundary conditions. For our case, these boundary conditions are the continuity of normal displacements and stresses and null tangential stresses on the two solid–fluid interfaces.

In order to establish the appropriate equation system, the incident field must be expressed in terms of waves centered on the axis of the circular cylindrical shell structure. This can be achieved with the aid of Graf's addition theorem, leading to the expression (in cylindrical coordinates):

$$\hat{\phi}_{\text{inc}} = -\frac{\mathrm{i}}{2} \sum_{n=0}^{\infty} (-1)^n \varepsilon_n H_n(k_{\alpha 1} r_0) J_n(k_{\alpha 1} r) \cos(n\theta) \, \mathrm{e}^{-\mathrm{i} k_{zm} z}, \tag{6}$$

where r_0 is the distance from the source to the axis of the circular shell.

The solution of the equation system can then be used to compute the stresses in the solid medium as a summation of solutions obtained for pairs of values of n and k_z. The final system of equations is presented in Appendix A.

4. Boundary element formulation

The BEM only requires the discretization of the internal and external boundaries of the shell. Detailed information on the BEM formulation applicable to the present problem can be found in Beskos [11].

The system of equations required for the solution is arranged so as to impose the continuity of the normal displacements, and normal stresses and null shear stresses along each interface between the fluid media and the shell structure. This system of equations requires the evaluation of the following integrals along the appropriately discretized boundaries:

$$H_{ij}^{(s)kl} = \int_{C_l} H_{ij}^{(s)}(x_k, x_l, n_l) \, \mathrm{d}C_l \quad (i, j = 1, 2, 3), \qquad H_{f1}^{(f)kl} = \int_{C_l} H_{f1}^{(f)}(x_k, x_l, n_l) \, \mathrm{d}C_l,$$

$$G_{ij}^{(s)kl} = \int_{C_l} G_{ij}^{(s)}(x_k, x_l) \, \mathrm{d}C_l \quad (i = 1, 2, 3; j = 1), \qquad G_{f1}^{(f)kl} = \int_{C_l} G_{f1}^{(f)}(x_k, x_l) \, \mathrm{d}C_l \tag{7}$$

in which $H_{ij}^{(s)}(x_k, x_l, n_l)$ and $G_{ij}^{(s)}(x_k, x_l)$ are the Green's tensor for traction and displacement components, respectively, in the elastic medium, at point x_l, in direction j, caused by a concentrated load acting at the source point x_k in direction i; $H_{f1}^{(f)}(x_k, x_l, n_l)$ are the components of the Green's tensor for pressure in the fluid medium, at point x_l, caused by a pressure load acting at the source point x_k; $G_{f1}^{(f)}(x_k, x_l)$ are the components of the Green's tensor for displacement in the fluid medium, at point x_l, in the normal direction, caused by a pressure load acting at the source point x_k; n_l is the unit outward normal for the lth boundary segment C_l; the subscripts $i, j = 1, 2, 3$ denote the normal, tangential and z-directions, respectively. These equations are conveniently transformed from the x, y, z Cartesian coordinate system by means of standard vector transformation operators. The required 2.5D fundamental solutions (Green's functions) in Cartesian co-ordinates, for the elastic and fluid media, are given below:

- Elastic medium:

$$G_{xx} = A\left[k_s^2 H_{0\beta} - \frac{1}{r}B_1 + \gamma_x^2 B_2\right], \qquad G_{yy} = A\left[k_s^2 H_{0\beta} - \frac{1}{r}B_1 + \gamma_y^2 B_2\right],$$

$$G_{zz} = A[k_s^2 H_{0\beta} - k_z^2 B_0], \qquad G_{xy} = G_{yx} = \gamma_x \gamma_y A B_2, \qquad G_{xz} = G_{zx} = \mathrm{i} k_z \gamma_x A B_1,$$

$$G_{yz} = G_{zy} = \mathrm{i} k_z \gamma_y A B_1, \tag{8}$$

where λ, μ are the Lamé constants; ρ the mass density; $\alpha = ((\lambda + 2\mu)/\rho)^{1/2}$ the P wave velocity; $\beta = (\mu/\rho)^{1/2}$ the S wave velocity; $k_p = \omega/\alpha$, $k_s = \omega/\beta$ the wave number; $k_\alpha = (k_p^2 - k_z^2)^{1/2}$, $k_\beta = (k_s^2 - k_z^2)^{1/2}$ the wave number;

$A = 1/4i\rho\omega^2$ the amplitude; $\gamma_i = \partial r/\partial x_i = x_i/r$ ($i = 1, 2$) the direction cosines; $H_{n\alpha} = H_n^{(2)}(k_\alpha r)$, $H_{n\beta} = H_n^{(2)}(k_\beta r)$ the Hankel functions; $B_n = k_\beta^n H_{n\beta} - k_\alpha^n H_{n\alpha}$ the B_n functions.

- Fluid media:

$$G_{fx} = -A_f k_{\alpha f} H_{1\alpha f}\gamma_x, \qquad G_{fy} = -A_f k_{\alpha f} H_{1\alpha f}\gamma_y, \tag{9}$$

where $k_{\alpha f} = (k_{pf}^2 - k_z^2)^{1/2}$ is the wave number; $A_f = 1/4i$ the amplitude; $H_{n\alpha f} = H_n^{(2)}(k_{\alpha f}r)$ the Hankel functions.
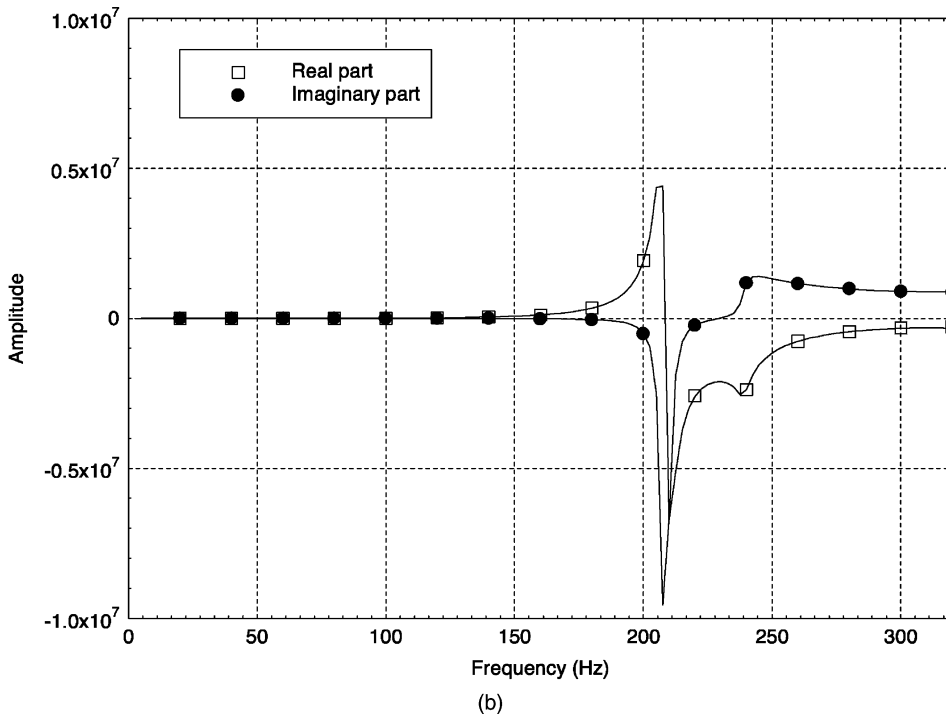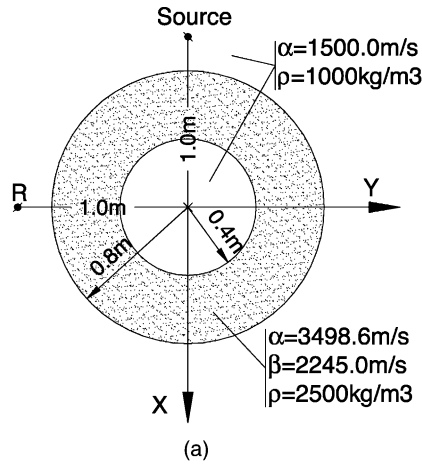

Fig. 3. Validation of the BEM algorithm: (a) geometry of the model; (b) response computed at receiver R.

The required integrations in Eq. (7) are performed analytically for the loaded element, and by using a Gaussian quadrature scheme when the element to be integrated is not the loaded element.

5. BEM validation

The results computed by the present BEM algorithm were compared with those obtained analytically using the formulation described above. Fig. 3a illustrates the geometry of the model used in the validation, assuming a cylindrical circular elastic shell structure, with an internal diameter of 0.8 m and an external diameter of 1.6 m, inserted in an infinite fluid medium. The mechanical properties of the elastic medium and those of the two fluids are listed in the same figure.

A spatially sinusoidal harmonic pressure line load is applied at $x = -1.0$ m and $y = 0.0$ m. Computations are achieved in the frequency domain [2.50, 320.0 Hz] with a frequency increment of 2.5 Hz.

Fig. 3b displays the real and imaginary parts of the scattered pressure field recorded by the receiver placed at $x = 0.0$ m and $y = -1.0$ m (labeled R), for a pressure line load with $k_z = 1.0$ rad/m. The solid lines represent the analytical solutions, while the marked line corresponds to the BEM solution. The square marks indicate the real part of the response, while the round marks refer to the imaginary part.

The results computed at receiver R enable one to conclude that the two solutions are in very close agreement, indicating that the BEM model is accurate. Equally good results were achieved from tests in which different loads and receivers were situated at different points.

6. Time responses

After obtaining frequency domain responses, the pressure in the spatial–temporal domain is computed by a numerical fast inverse Fourier transform in ω. For this purpose, the pressure point source is assumed to have a temporal variation defined by a Ricker pulse. In the frequency domain, this pulse is defined as

$$U(\omega) = A \left[2\sqrt{\pi} t_0 \, e^{-i\omega t_s} \right] \Omega^2 \, e^{-\Omega^2} \tag{10}$$

in which $\Omega = \omega t_0/2$, t denotes time and πt_0 the characteristic (dominant) period of the wavelet.

This technique allows analyses for a total time window of $T = 2\pi/\Delta\omega$, where $\Delta\omega$ is the frequency step. Pulses arriving at times later than T will appear again in the beginning of this window, generating the so-called aliasing phenomenon. To avoid the contribution of these pulses, complex frequencies of the form $\omega_c = \omega - i\eta$ (with $\eta = 0.7\Delta\omega$) are used (e.g. [12]). In the time domain, this shift is taken into account by applying an exponential window $e^{\eta t}$ to the response [13].

7. Numerical examples

All the examples given here have a cylindrical shell structure defined by two circular cylindrical surfaces. The inner surface has a diameter of 1.00 m while that of the outer surface is 1.40 m. Each surface is modeled using 150 boundary elements. This structure is submerged in a fluid medium, which allows a pressure wave propagation velocity of 1500 m/s and exhibits a density of $\rho = 1000$ kg/m^3. The fluid filling the shell is assumed to have the same properties as the host medium, while the elastic material of the shell structure is concrete, with a Poisson ratio of $\nu = 0.15$, a density of $\rho = 2500$ kg/m^3 and Young's modulus $E = 29.0$ GPa, allowing propagation velocities for the P and S waves of 3498.6 and 2245.0 m/s, respectively. Pressure responses are calculated at four sets of receivers placed in the fluid filling the structure. Each set consists of a line of five receivers, placed along the z-direction and with different z-coordinates. The z-coordinate of each receiver is indicated in the time responses.
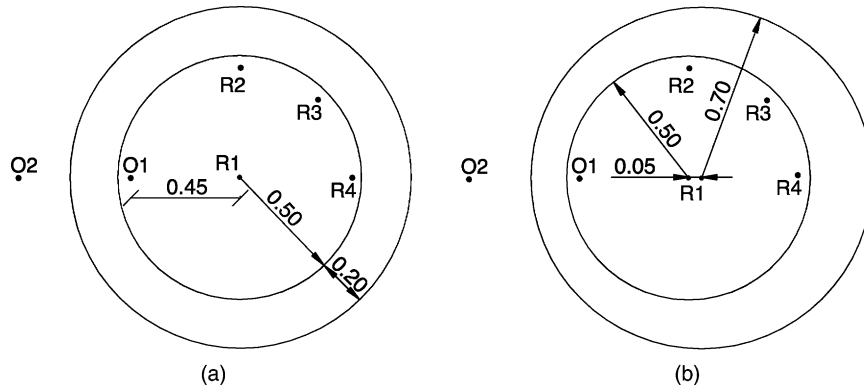
Fig. 4. Geometry of the model: (a) case 1; (b) case 2.

Two distinct situations are simulated, as shown in Fig. 4. The first corresponds to a cylindrical shell structure defined by two concentric circumferences, with a constant wall thickness of 0.20 m (case 1, Fig. 4a). In the second situation, the cylindrical shell structure is assumed to have a construction defect; thus, two non-concentric circumferences define the structure, with their centers placed 0.05 m apart (case 2, Fig. 4b). For both cases, point pressure loads, placed either inside (position O1) or outside (position O2) the structure, illuminate the dynamic system. The 3D response is given by a discrete summation of 2.5D responses, as described in Section 2.

All the computations were performed for frequencies in the range of 8–1024 Hz, with increments of 8 Hz. This frequency step determines a maximum time analysis of 0.125 ms for the time domain responses. The time domain responses presented are computed by means of an inverse Fourier transformation, assuming the source generates a Ricker pulse with a central frequency of 350.0 Hz.

7.1. Case 1—cylindrical shell structure with cross-section defined by two concentric circumferences

Fig. 5a displays both the frequency vs. phase velocity and the time domain pressures responses computed at receivers R1, when a point pressure load is excited at position O1, within the case 1 structure. The response in the frequency vs. phase velocity domain is determined by computing the solution of the problem for different values of the parameter $k_z = \omega/c$, with c being the apparent wave velocity along z. For these figures to be understood more easily, the frequency vs. phase velocity responses only represent phase velocities ranging from 800.0 to 1600.0 m/s. The response registered for higher phase velocities is omitted in these figures. However, time responses are calculated for the full range of velocities, and thus they take into account the contribution of all waves involved.

The response registered at receivers R1 (Fig. 5a), placed over the geometric center of the system, reveals the existence of different types of waves. In the frequency vs. phase velocity response, waves traveling in the fluid with the pressure wave propagation velocity of 1500.0 m/s are clearly visible (labeled "F"). An additional excited mode can also be seen (labeled as "A0"). This mode corresponds to dispersive guided waves, exhibiting phase velocities below the fluid pressure wave velocity. It seems to exist in the full frequency range. Its mode shape was computed over a fine grid of receivers placed inside the structure, for frequencies of $f = 200.0$ Hz ($c = 1200.0$ m/s), $f = 350.0$ Hz ($c = 1132.0$ m/s) and $f = 1000.0$ Hz ($c = 996.0$ m/s), illustrated in Fig. 5b. In Fig. 5a, a pair of numbers identifies the frequency position of each of these points (Aij), the first number identifying the azimuthal order of the mode and the second giving its relative position in the frequency domain. For this case, it clearly indicates that this is an axisymmetric mode and its shape remains constant with the frequency variation.

The features described can also be identified in the time domain responses of Fig. 5a. A pulse can be detected in the time responses, corresponding to waves traveling with the fluid velocity, and labeled as "PF". There follows a dense ring of pulses associated with the "A0" normal mode (labeled "PA0"). Since "A0" is a highly dispersive
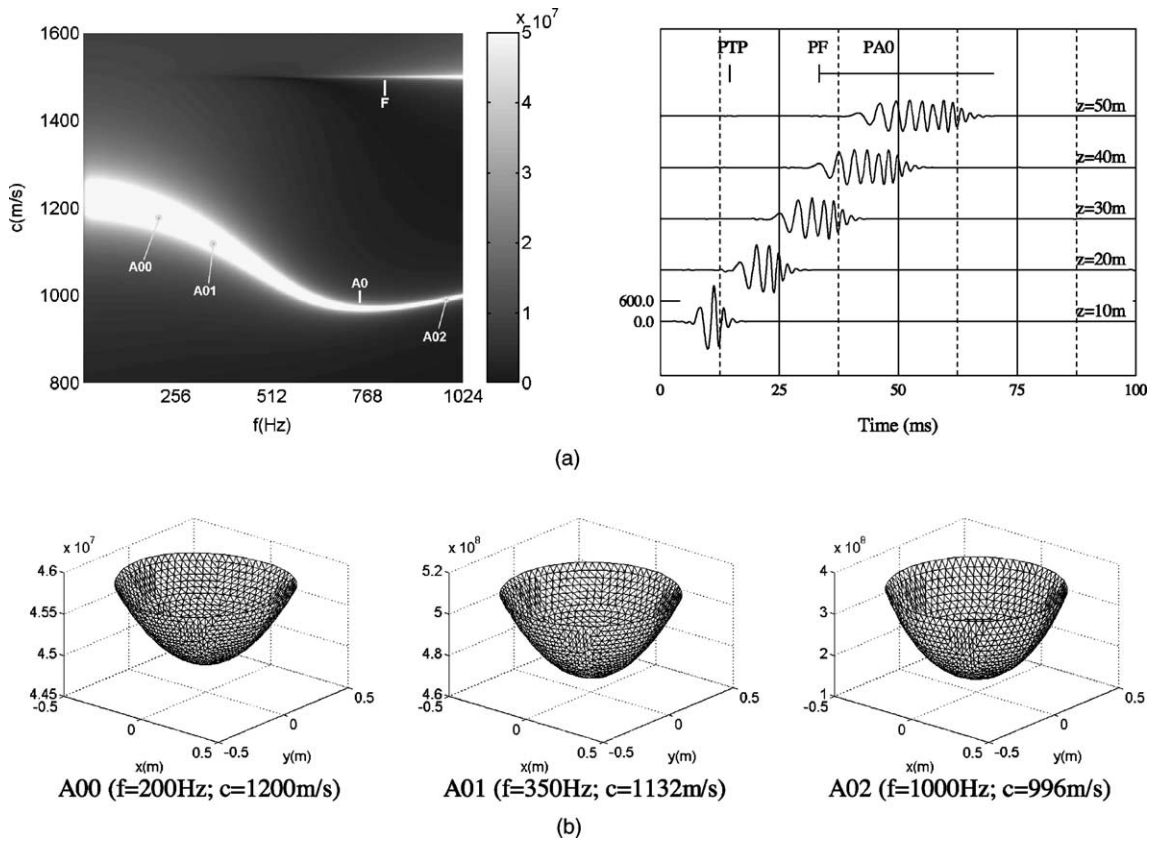
Fig. 5. Cylindrical shell structure defined by two concentric circumferences: (a) frequency vs. phase velocity and time responses at receivers R1 due to a point source located at O1; (b) pressure response across the fluid filling the structure along "A0".

mode, its contribution appears in the time response as a sequence of pulses that start to arrive after the waves that travel with the pressure wave velocity of the fluid. The time responses show that there is a third type of pulse, labeled "PTP", in this system. It exhibits higher propagation velocities and is associated with waves that exist in thin plates and shells. These waves could not be identified in the frequency responses due to the range of phase velocities shown. According to Graff [14], this "thin-plate velocity" is given by $(E/(1 - v^2)\rho)^{1/2}$. The mechanical properties ascribed to the elastic medium allow the "thin-plate velocity" to be approximately 3445 m/s. The calculation using this expression does not take into account the solid/fluid coupling, and thus there is a discrepancy between this result and the group velocities registered in the time responses ($\approx$3350 m/s).

The R1 receivers only register the influence of the "A0" normal mode. However, other guided modes may be excited in this system, some of them exhibiting an azimuthal variation. We have referred to them as "An", where n indicates the variation of the mode with azimuth. The response computed at receiver R2 (Fig. 6a), reveals one of these modes. It is highly dispersive, and the mode shape computed at frequencies $f = 200.0$ Hz ($c = 1490.0$ m/s), $f = 350.0$ Hz ($c = 934.0$ m/s) and $f = 1000.0$ Hz ($c = 1074.0$ m/s) (see Fig. 6b) shows that it is a normal mode with azimuthal variation of second order, corresponding to screw waves (identified as "A2"). It was not recorded at receivers R1 since these receivers were placed over its nodal line. Time responses reveal the existence of these identified wave types, with the additional contribution of pulses traveling with the so-called "thin-plate velocity" (labeled "PTP"). The presence of pulses related to the "A2" normal mode are harder to identify, since they appear as being superimposed on those related to the "A0" mode, which dominates the response.
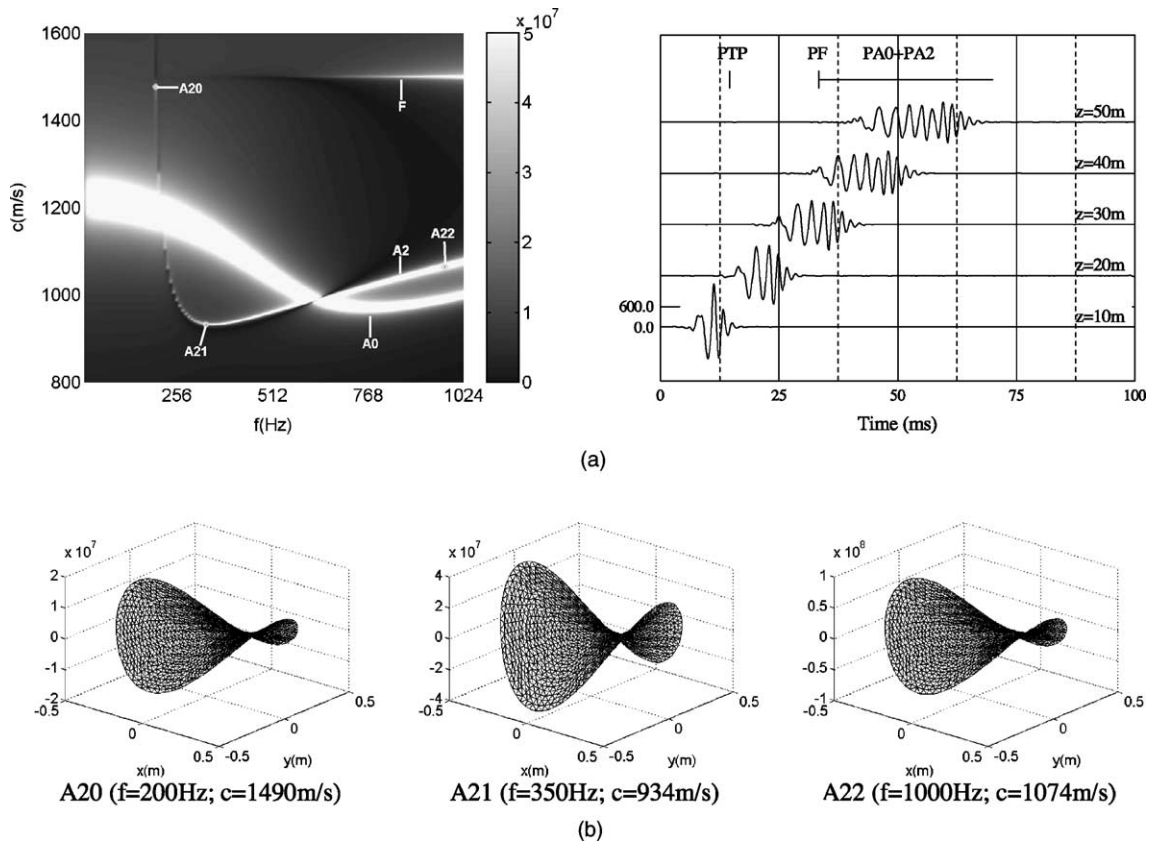
Fig. 6. Cylindrical shell structure defined by two concentric circumferences: (a) frequency vs. phase velocity and time responses at receivers R2 due to a point source located at O1; (b) pressure response across the fluid filling the structure along "A2".

The response computed at receivers R3 is represented in Fig. 7. One axisymmetric mode (labeled "A0") and two normal modes with azimuthal variation are registered at this position (labeled "A1" and "A3"), while the "A2" mode noted earlier is not visible. Observing the mode shapes A1 computed for frequencies $f = 200.0$ Hz ($c = 894.0$ m/s), $f = 350.0$ Hz ($c = 986.0$ m/s) and $f = 1000.0$ Hz ($c = 1014.0$ m/s), and mode shapes calculated for A3 at $f = 704.0$ Hz ($c = 1368.0$ m/s), $f = 850.0$ Hz ($c = 1288.0$ m/s) and $f = 1000.0$ Hz ($c = 1264.0$ m/s) (Fig. 7b), it may be concluded that these "A1" and "A3" modes could not be seen at receivers R1 and R2 since the receivers were over the nodal line of these modes. The absence of "A2" waves is similarly explained, since they make null contribution for receivers placed over lines that pass through the center of the structure and form an angle of $45°$ with the horizontal axis. Notice that, as before, the shape of the A1 and A3 modes remained constant as the frequency varies. The time responses allow the identification of some of the features described for the frequency response. The arrival times of the waves traveling with the "thin-plate velocity" and with the fluid pressure wave velocity can be identified. It is then possible to observe the arrival of a sequence of waves that correspond to the normal modes excited. The time responses register a significant pressure variation after the arrival of the waves associated with the "A0", "A1" modes, which is generated by the mode "A3", given its low group velocity. This mode also exhibits a clear cutoff frequency around $f = 500.0$ Hz.

All the modes described above ("A0", "A1", "A2" and "A3") are visible at receivers R4, as shown in the frequency vs. phase velocity and time responses in Fig. 8. The amplitude of the non-axisymmetric modes seems to increase, since the "A1", "A2" and "A3" modes reach all maximum amplitudes at this position. The time domain response
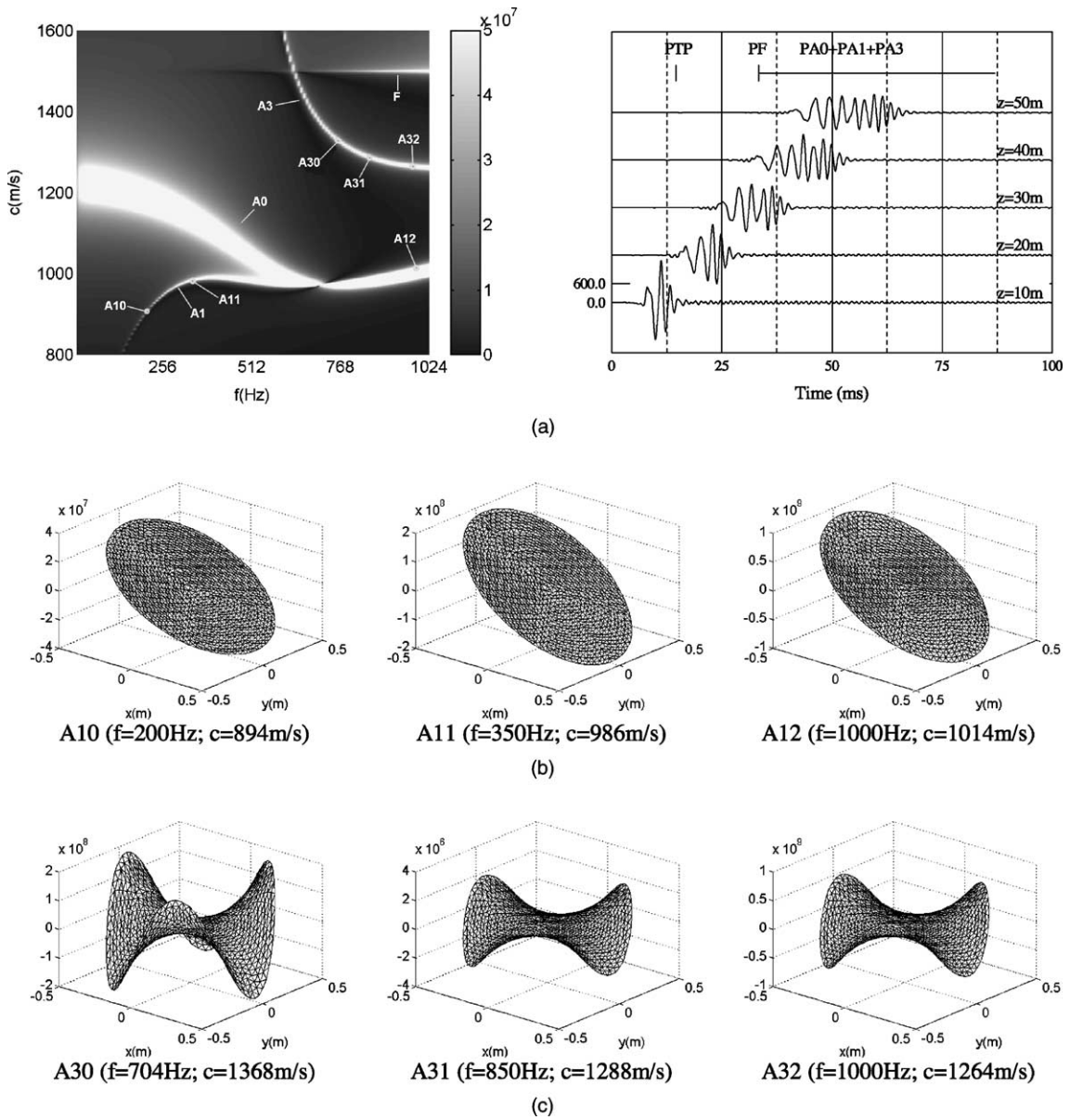
Fig. 7. Cylindrical shell structure defined by two concentric circumferences: (a) frequency vs. phase velocity and time responses at receivers R3 due to a point source located at O1; (b) pressure response across the fluid filling the structure along "A1"; (c) pressure response across the fluid filling the structure along "A3".

reveals all the features identified before, with the arrival of the "PTP" and "PF" pulses followed by a sequence of waves corresponding to normal modes. This time domain response is very similar to that obtained at receivers R1, R2 and R3. However, this happens because the amplitude of the "A0" mode, visible at all receivers, appears to dominate the overall amplitude of the response.

The same model has been subjected to a point load placed at position O2, outside the shell structure. Fig. 9 illustrates the frequency and time domain responses computed at receivers R4. The main features found for the point
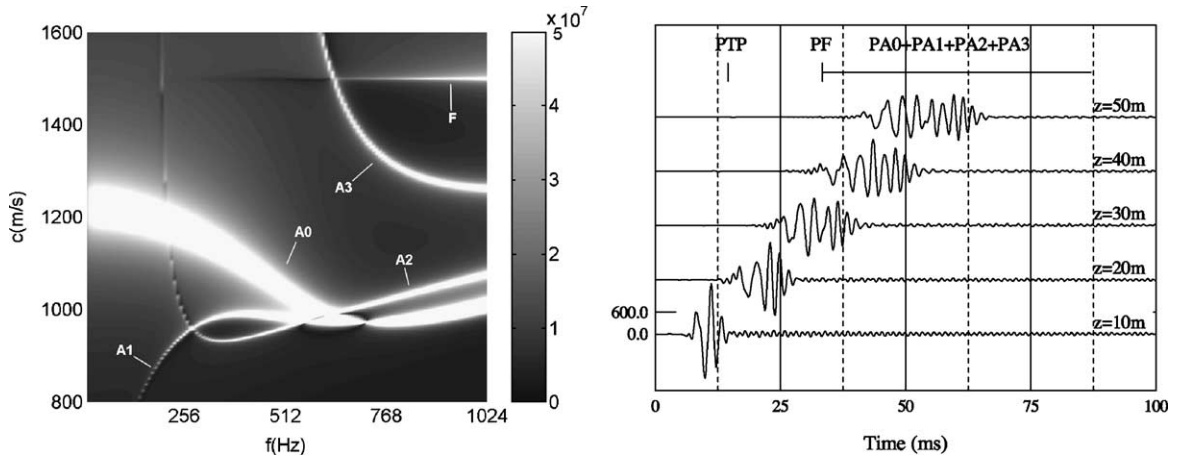
Fig. 8. Frequency vs. phase velocity and time responses at receivers R4 due to a point source located at O1 in the vicinity of a cylindrical shell structure defined by two concentric circumferences.

source located at O1 can still be identified. However, there is a global decrease in the amplitude of the response, mainly due to the diminished importance of the "A0" mode. The time responses further confirm this behavior, by exhibiting lower amplitude after the arrival of the pulses associated with waves traveling at the "thin-plate velocity" (PTP) and at the pressure wave velocity (PF).

7.2. Case 2—cylindrical shell structure with cross-section defined by two non-concentric circumferences

In order to understand the effect of a construction defect on the final dynamic response of the system, simulation analyses were performed using the case 2 model.

The pressures in the frequency vs. phase velocity and in the time domain computed at receivers R1 when the surfaces defining the shell are not concentric and the source is at position O1 are given in Fig. 10a. In the frequency
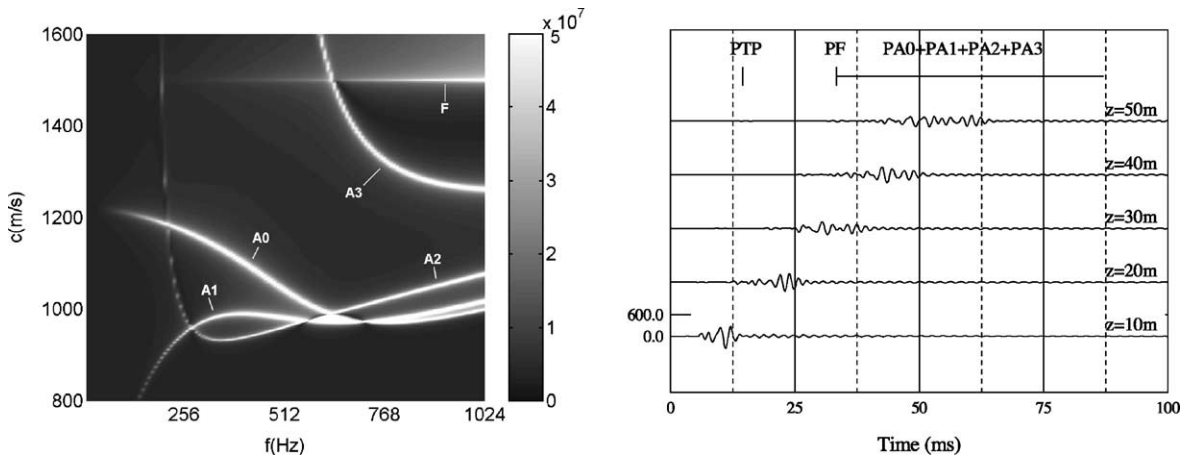

Fig. 9. Frequency vs. phase velocity and time responses at receivers R4 due to a point source located at O2 in the vicinity of a cylindrical shell structure defined by two concentric circumferences.

vs. phase velocity domain, the presence of waves associated with the pressure velocity of the fluid (F) can still be easily identified. The response registered at the same receivers also exhibits, as before, different dispersive guided waves that generate an enhancement of the response along well-defined lines in the frequency vs. phase velocity plots. Four lines are visible and labeled "Li" ($i = 0, 3$). Fig. 10b–e plot the pressure at a fine grid of receivers placed
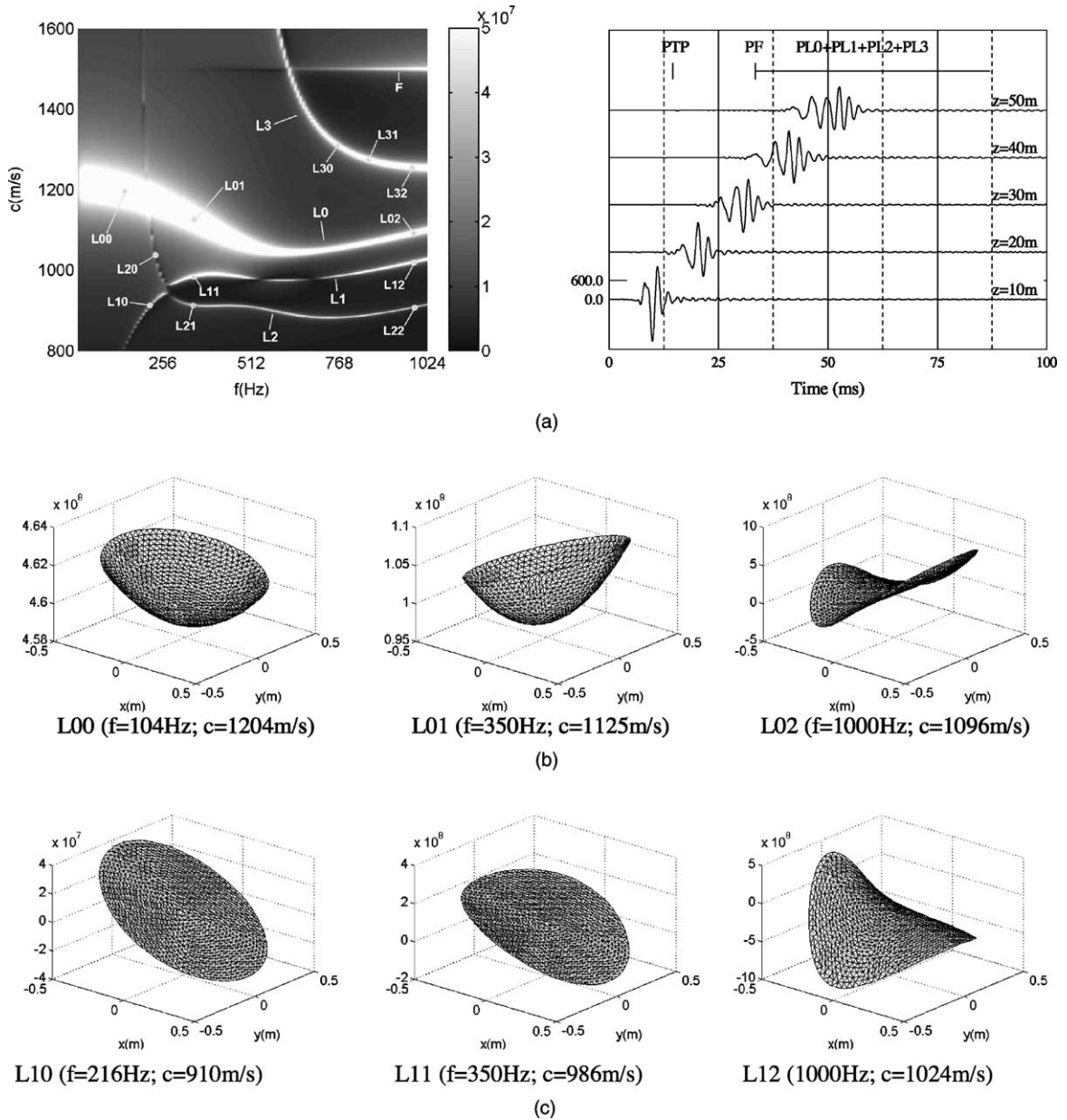

Fig. 10. Cylindrical shell structure defined by two non-concentric circumferences: (a) frequency vs. phase velocity and time responses at receivers R4 due to a point source located at O1; (b) pressure response across the fluid filling the structure along line L0; (c) pressure response across the fluid filling the structure along line L1; (d) pressure response across the fluid filling the structure along line L2; (e) pressure response across the fluid filling the structure along line L3.
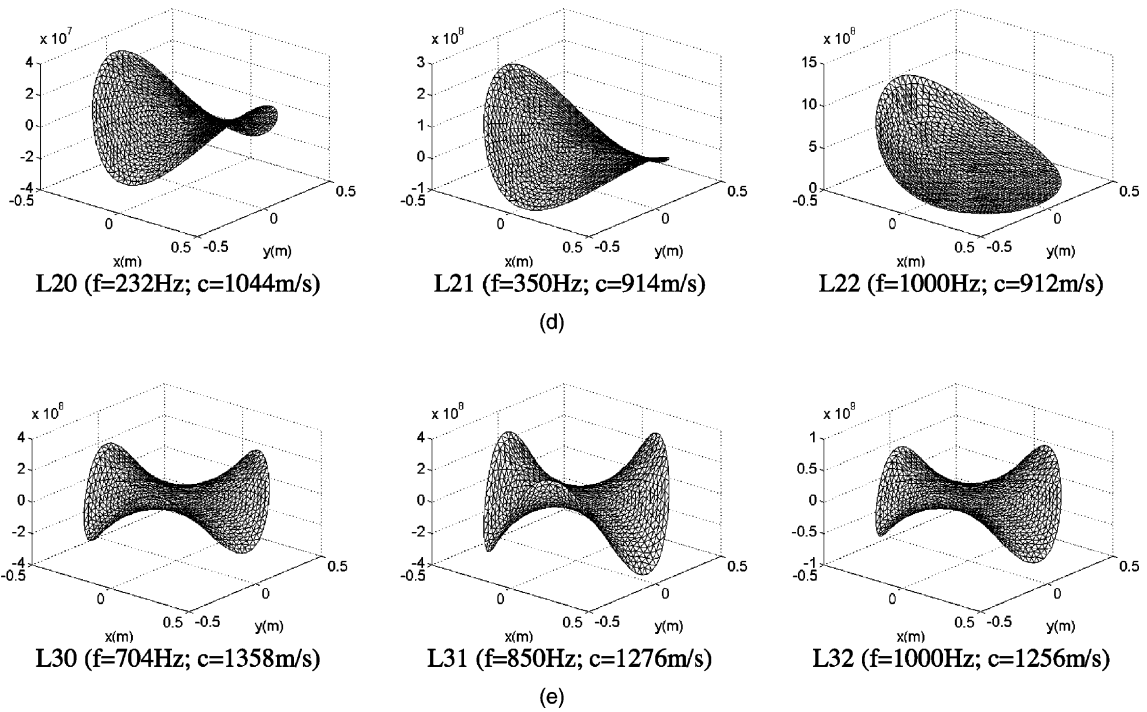
L20 (f=232Hz; c=1044m/s)   L21 (f=350Hz; c=914m/s)   L22 (f=1000Hz; c=912m/s)

(d)

L30 (f=704Hz; c=1358m/s)   L31 (f=850Hz; c=1276m/s)   L32 (f=1000Hz; c=1256m/s)

(e)

Fig. 10. (*continued*).

in the inner fluid along each of those lines (L*i*) for different frequencies. A pair of numbers identifies each plot: the first number identifies the line while the second gives the relative position in the frequency domain. Analysis of these plots shows that along each line, the shape of the response does not remain constant as the frequency changes. At low frequencies, the response appears to behave like the modes defined for case 1. Indeed, at low frequencies, it is possible to detect the mode shapes defined by the A0, A1 and A2 modes. Meanwhile, the plots defining the L3 response appear to keep the mode shape of A3 in the vicinity of its cutoff frequency. As the frequency increases, the shape of the computed pressure responses changes significantly, apparently as a result of a combination of different behaviors corresponding to the previously computed "A*i*" modes.

Analyzing the responses registered at the different lines, "L*i*", it can be confirmed that the guided waves associated with "L0" exhibit higher amplitudes. The response associated with this line is seen to be less dispersive than the "A0" line of case 1. The time response corroborates this behavior, as the ring of pulses associated with larger amplitude guided waves stops arriving earlier than before.

Frequency vs. phase velocity and time domain responses have also been computed at receivers R1, R2 and R3, as illustrated in Fig. 11. The frequency response at receivers R1 (Fig. 11a) clearly shows that the "L0" line dominates the response. At low frequencies, lines "L1" and "L2" register only low amplitude responses. It should be noted that, at these frequencies, the case 1 model exhibited null contribution of the corresponding normal modes ("A1" and "A2"). However, in case 2 the receiver R1 is no longer placed over an axis of axisymmetry, and thus may register a small contribution of non-axisymmetric wave modes. It is also possible to observe that the response related to line "L3" is now very low, especially near its cutoff frequency. In the time domain, pulses arriving at the end of the time window, observed at receivers R4, are no longer visible at this receiver, due to the small contribution of waves traveling with very low velocities and associated with line "L3".

In the response registered at receiver R2 (Fig. 11b) it is possible to observe that the contribution of waves associated with the line "L2" is now significant at low frequencies. In fact, at these frequencies the computed mode shape of
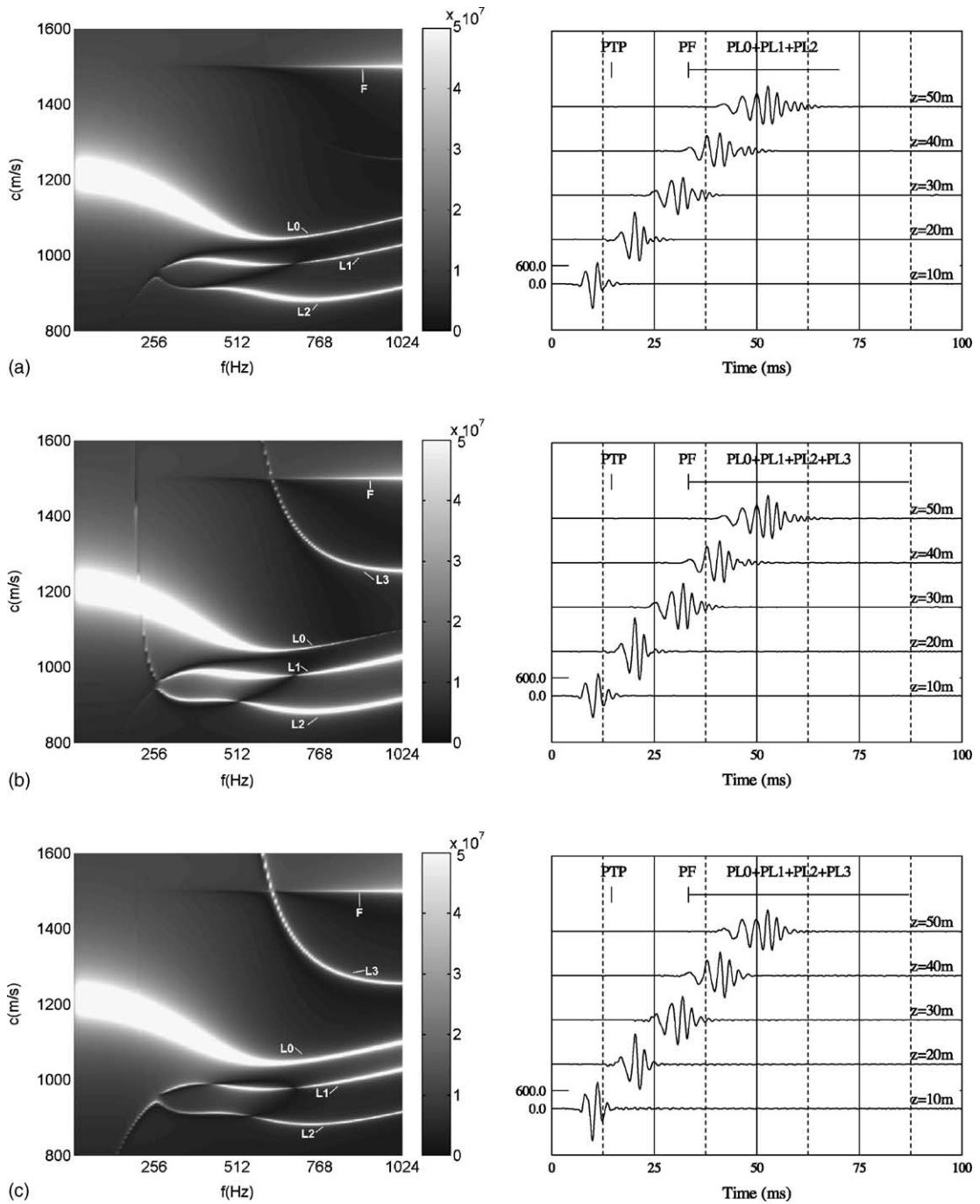
Fig. 11. Frequency and time domain response computed for case 2 due to a point source located at O1: (a) receivers R1; (b) receivers R2; (c) receivers R3.

"L2" is very similar to the "A2" mode of case 1, reaching maximum amplitude at this receiver. Furthermore, the contribution of waves associated with the response line "L3" is now more evident, in particular at frequencies closer to the cutoff frequency of this line. The time response is very similar to that observed at R1, with pulses arriving at later times, associated with the "L3" line having a slight amplitude increase.

At receivers R3 (Fig. 11c), it can be seen that the line "L2" shows very low amplitudes at low frequencies, while the importance of the "L1" line seems to increase. Again, this behavior was expected, since for low frequencies these lines approach the case 1 mode shape of the "A2" and "A1" modes, respectively. The amplitude of the "L3" response line is also greatly enhanced at this receiver. The time response further confirms this behavior, with pulses arriving at later times appearing with higher amplitudes.

Simulations were also performed for the same model, assuming the excitation source to be placed at position O2 (not shown). As in case 1, the main features described when the point source was located at O1 can still be identified. Both frequency and time responses reveal a global fall in amplitude, which is even more evident than in case 1. In the time domain, the pulses associated with waves traveling with the "thin-plate velocity" (PTP), with the pressure wave velocity (PF) and with the normal modes excited (Li) can be identified.

8. Conclusions

The pressure inside an infinite cylindrical shell structure, submerged in a homogeneous fluid medium, and subjected to the incidence of waves generated by a point pressure load, has been computed. The structure was modeled as an elastic material, and the full interaction between the two fluids and the structure was taken into account. Two different models were analyzed, corresponding to shell structures defined by two concentric or non-concentric circumferences. Results were obtained in both the frequency and time domains, allowing the main features of the wave propagation to be identified.

The results obtained when the inner and outer surfaces are defined by two concentric circumferences reveal that multiple normal modes are excited and their contribution to the response depends on the position of the receiver. The different normal modes excited were clearly identified and their mode shape was computed, revealing a constant behavior with the frequency variation.

When the structure is defined by non-concentric circular surfaces, the pressure response in the frequency vs. phase velocity domain allowed the identification of well defined lines where the response exhibits higher amplitudes. At low frequencies and near the cutoff frequencies of these lines, the behavior of the response seems to approach that of the normal modes identified when the circumferences defining the inner and outer surfaces of the shell are concentric. However, as the frequency increases, the mode shapes computed indicate that the pressure response results from a combination of the different types of guided waves generated when the structure is defined by two concentric circumferences. This can be seen in both the frequency and time domains, and for the different receivers and source positions analyzed.

Appendix A

The eight potentials defined before allow the definition of a system of eight equations for eight unknowns, to yield the coefficients A_n^i ($i = 1, \ldots, 8$). The equation system is built so as to allow the establishment of boundary conditions of null tangential stresses and the continuity of normal displacements and stresses in the solid–fluid interfaces:

$$\begin{bmatrix} a_{11} & \ldots & a_{18} \\ \vdots & & \vdots \\ a_{81} & \ldots & a_{88} \end{bmatrix} \begin{bmatrix} A_n^1 \\ \vdots \\ A_n^8 \end{bmatrix} = \begin{bmatrix} b_1 \\ \vdots \\ b_8 \end{bmatrix}.$$

Assuming the outer and inner fluids to have Lamé constants λ_1 and λ_2, respectively, and the solid medium to have a shear modulus μ_2, the terms a_{ij} are defined as

Outer boundary:

$$a_{11} = \lambda_1(k_{\alpha 1}^2 + k_z^2)H_n^{(2)}(k_{\alpha 1}r_B),$$

$$a_{12} = \frac{2\mu_2}{r_B^2}\left[\left(n^2 - n - \frac{\omega^2 r_B^2}{2\beta_2^2} + k_z^2 r_B^2\right)J_n(k_{\alpha 2}r_B) + (k_{\alpha 2}r_B)J_{n+1}(k_{\alpha 2}r_B)\right],$$

$$a_{13} = \frac{2\mu_2}{r_B^2}[(-n + n^2)J_n(k_{\beta 2}r_B) - (nk_{\beta 2}r_B)J_{n+1}(k_{\beta 2}r_B)],$$

$$a_{14} = -ik_z\frac{2\mu_2}{r_B^2}[(-n + n^2 - k_{\beta 2}^2 r_B^2)J_n(k_{\beta 2}r_B) + (k_{\beta 2}r_B)J_{n+1}(k_{\beta 2}r_B)],$$

$$a_{15} = \frac{2\mu_2}{r_B^2}\left[\left(n^2 - n - \frac{\omega^2 r_B^2}{2\beta_2^2} + k_z^2 r_B^2\right)H_n^{(2)}(k_{\alpha 2}r_B) + (k_{\alpha 2}r_B)H_{n+1}^{(2)}(k_{\alpha 2}r_B)\right],$$

$$a_{16} = \frac{2\mu_2}{r_B^2}[(-n + n^2)H_n^{(2)}(k_{\beta 2}r_B) - (nk_{\beta 2}r_B)H_{n+1}^{(2)}(k_{\beta 2}r_B)],$$

$$a_{17} = -ik_z\frac{2\mu_2}{r_B^2}[(-n + n^2 - k_{\beta 2}^2 r_B^2)H_n^{(2)}(k_{\beta 2}r_B) + (k_{\beta 2}r_B)H_{n+1}^{(2)}(k_{\beta 2}r_B)],$$

$$a_{18} = 0, \qquad a_{21} = 0, \qquad a_{22} = [(n - n^2)J_n(k_{\alpha 2}r_B) + (nk_{\alpha 2}r_B)J_{n+1}(k_{\alpha 2}r_B)],$$

$$a_{23} = \left[\left(n - n^2 + \frac{k_{\beta 2}^2 r_B^2}{2}\right)J_n(k_{\beta 2}r_B) + (-k_{\beta 2}r_B)J_{n+1}(k_{\beta 2}r_B)\right],$$

$$a_{24} = -nik_z[(-n + 1)J_n(k_{\beta 2}r_B) + (k_{\beta 2}r_B)J_{n+1}(k_{\beta 2}r_B)],$$

$$a_{25} = [(n - n^2)H_n^{(2)}(k_{\alpha 2}r_B) + (nk_{\alpha 2}r_B)H_{n+1}^{(2)}(k_{\alpha 2}r_B)],$$

$$a_{26} = \left[\left(n - n^2 + \frac{k_{\beta 2}^2 r_B^2}{2}\right)H_n^{(2)}(k_{\beta 2}r_B) + (-k_{\beta 2}r_B)H_{n+1}^{(2)}(k_{\beta 2}r_B)\right],$$

$$a_{27} = -nik_z[(-n + 1)H_n^{(2)}(k_{\beta 2}r_B) + (k_{\beta 2}r_B)H_{n+1}^{(2)}(k_{\beta 2}r_B)],$$

$$a_{28} = 0, \qquad a_{31} = 0, \qquad a_{32} = -ik_z[(nr_B)J_n(k_{\alpha 2}r_B) - (k_{\alpha 2}r_B^2)J_{n+1}(k_{\alpha 2}r_B)],$$

$$a_{33} = \left[\frac{-ik_z}{2}nr_B J_n(k_{\beta 2}r_B)\right], \qquad a_{34} = \left\{\frac{1}{2r_B}(k_{\beta 2}^2 r_B^2 - k_z^2 r_B^2)[nJ_n(k_{\beta 2}r_B) - (k_{\beta 2}r_B)J_{n+1}(k_{\beta 2}r_B)]\right\},$$

$$a_{35} = -ik_z[(nr_B)H_n^{(2)}(k_{\alpha 2}r_B) - (k_{\alpha 2}r_B^2)H_{n+1}^{(2)}(k_{\alpha 2}r_B)], \qquad a_{36} = \left[\frac{-ik_z}{2}nr_B H_n^{(2)}(k_{\beta 2}r_B)\right],$$

$$a_{37} = \left\{\frac{1}{2r_B}(k_{\beta 2}^2 r_B^2 - k_z^2 r_B^2)[nH_n^{(2)}(k_{\beta 2}r_B) - (k_{\beta 2}r_B)H_{n+1}^{(2)}(k_{\beta 2}r_B)]\right\}, \qquad a_{38} = 0,$$

$$a_{41} = -\left[\frac{n}{r_B}H_n^{(2)}(k_{\alpha 1}r_B) - k_{\alpha 1}H_{n+1}^{(2)}(k_{\alpha 1}r_B)\right], \qquad a_{42} = \left[\frac{n}{r_B}J_n(k_{\alpha 2}r_B) - k_{\alpha 2}J_{n+1}(k_{\alpha 2}r_B)\right],$$

$$a_{43} = \left[\frac{n}{r_B}J_n(k_{\beta 2}r_B)\right], \qquad a_{44} = -ik_z\left[\frac{n}{r_B}J_n(k_{\beta 2}r_B) - k_{\beta 2}J_{n+1}(k_{\beta 2}r_B)\right],$$

$$a_{45} = \left[\frac{n}{r_B}H_n^{(2)}(k_{\alpha 2}r_B) - k_{\alpha 2}H_{n+1}^{(2)}(k_{\alpha 2}r_B)\right], \qquad a_{46} = \left[\frac{n}{r_B}H_n^{(2)}(k_{\beta 2}r_B)\right],$$

$$a_{47} = -ik_z\left[\frac{n}{r_B}H_n^{(2)}(k_{\beta 2}r_B) - k_{\beta 2}H_{n+1}^{(2)}(k_{\beta 2}r_B)\right], \qquad a_{48} = 0.$$

Inner boundary:

$$a_{51} = 0, \qquad a_{52} = \frac{2\mu_2}{r_A^2}\left[\left(n^2 - n - \frac{\omega^2 r_A^2}{2\beta_2^2} + k_z^2 r_A^2\right)J_n(k_{\alpha2}r_A) + (k_{\alpha2}r_A)J_{n+1}(k_{\alpha2}r_A)\right],$$

$$a_{53} = \frac{2\mu_2}{r_A^2}[(-n+n^2)J_n(k_{\beta2}r_A) - (nk_{\beta2}r_A)J_{n+1}(k_{\beta2}r_A)],$$

$$a_{54} = -\mathrm{i}k_z\frac{2\mu_2}{r_A^2}[(-n+n^2-k_{\beta2}^2r_A^2)J_n(k_{\beta2}r_A) + (k_{\beta2}r_A)J_{n+1}(k_{\beta2}r_A)],$$

$$a_{55} = \frac{2\mu_2}{r_A^2}\left[\left(n^2 - n - \frac{\omega^2 r_A^2}{2\beta_2^2} + k_z^2 r_A^2\right)H_n^{(2)}(k_{\alpha2}r_A) + (k_{\alpha2}r_A)H_{n+1}^{(2)}(k_{\alpha2}r_A)\right],$$

$$a_{56} = \frac{2\mu_2}{r_A^2}[(-n+n^2)H_n^{(2)}(k_{\beta2}r_A) - (nk_{\beta2}r_A)H_{n+1}^{(2)}(k_{\beta2}r_A)],$$

$$a_{57} = -\mathrm{i}k_z\frac{2\mu}{r_A^2}[(-n+n^2-k_{\beta2}^2r_A^2)H_n^{(2)}(k_{\beta2}r_A) + (k_{\beta2}r_A)H_{n+1}^{(2)}(k_{\beta2}r_A)],$$

$$a_{58} = \lambda_2(k_{\alpha2}^2 + k_z^2)J_n(k_{\alpha2}r_A), \qquad a_{61} = 0, \qquad a_{62} = [(n-n^2)J_n(k_{\alpha2}r_A) + (nk_{\alpha2}r_A)J_{n+1}(k_{\alpha2}r_A)],$$

$$a_{63} = \left[\left(n - n^2 + \frac{k_{\beta2}^2 r_A^2}{2}\right)J_n(k_{\beta2}r_A) + (-k_{\beta2}r_A)J_{n+1}(k_{\beta2}r_A)\right],$$

$$a_{64} = -n\mathrm{i}k_z[(-n+1)J_n(k_{\beta2}r_A) + (k_{\beta2}r_A)J_{n+1}(k_{\beta2}r_A)],$$

$$a_{65} = [(n-n^2)H_n^{(2)}(k_{\alpha2}r_A) + (nk_{\alpha2}r_A)H_{n+1}^{(2)}(k_{\alpha2}r_A)],$$

$$a_{66} = \left[\left(n - n^2 + \frac{k_{\beta2}^2 r_A^2}{2}\right)H_n^{(2)}(k_{\beta2}r_A) + (-k_{\beta2}r_A)H_{n+1}^{(2)}(k_{\beta2}r_A)\right],$$

$$a_{67} = -n\mathrm{i}k_z[(-n+1)H_n^{(2)}(k_{\beta2}r_A) + (k_{\beta2}r_A)H_{n+1}^{(2)}(k_{\beta2}r_A)],$$

$$a_{68} = 0, \qquad a_{71} = 0,$$

$$a_{72} = -\mathrm{i}k_z[(nr_A)J_n(k_{\alpha2}r_A) - (k_{\alpha2}r_A^2)J_{n+1}(k_{\alpha2}r_A)],$$

$$a_{73} = \left[\frac{-\mathrm{i}k_z}{2}nr_A J_n(k_{\beta2}r_A)\right], \qquad a_{74} = \left\{\frac{1}{2r_A}(k_{\beta2}^2r_A^2 - k_z^2 r_A^2)[nJ_n(k_{\beta2}r_A) - (k_{\beta2}r_A)J_{n+1}(k_{\beta2}r_A)]\right\},$$

$$a_{75} = -\mathrm{i}k_z[(nr_A)H_n^{(2)}(k_{\alpha2}r_A) - (k_{\alpha2}r_A^2)H_{n+1}^{(2)}(k_{\alpha2}r_A)], \qquad a_{76} = \left[\frac{-\mathrm{i}k_z}{2}nr_A H_n^{(2)}(k_{\beta2}r_A)\right],$$

$$a_{77} = \left\{\frac{1}{2r_A}(k_{\beta2}^2r_A^2 - k_z^2 r_A^2)[nH_n^{(2)}(k_{\beta2}r_A) - (k_{\beta2}r_A)H_{n+1}^{(2)}(k_{\beta2}r_A)]\right\},$$

$$a_{78} = 0, \qquad a_{81} = 0, \qquad a_{82} = \left[\frac{n}{r_A}J_n(k_{\alpha2}r_A) - k_{\alpha2}J_{n+1}(k_{\alpha2}r_A)\right], \qquad a_{83} = \left[\frac{n}{r_A}J_n(k_{\beta2}r_A)\right],$$

$$a_{84} = -\mathrm{i}k_z\left[\frac{n}{r_A}J_n(k_{\beta2}r_A) - k_{\beta2}J_{n+1}(k_{\beta2}r_A)\right], \qquad a_{85} = \left[\frac{n}{r_A}H_n^{(2)}(k_{\alpha2}r_A) - k_{\alpha2}H_{n+1}^{(2)}(k_{\alpha2}r_A)\right],$$

$$a_{86} = \left[\frac{n}{r_A}H_n^{(2)}(k_{\beta2}r_A)\right], \qquad a_{87} = -\mathrm{i}k_z\left[\frac{n}{r_A}H_n^{(2)}(k_{\beta2}r_A) - k_{\beta2}H_{n+1}^{(2)}(k_{\beta2}r_A)\right],$$

$$a_{88} = -\left[\frac{n}{r_A}J_n(k_{\alpha2}r_A) - k_{\alpha2}J_{n+1}(k_{\alpha2}r_A)\right].$$

For a pressure source located in the outer fluid, the terms b_j are defined as

$$b_1 = \frac{i}{2}\varepsilon_n(-1)^n H_n^{(2)}(k_{\alpha 1}r_0)\lambda_{f1}\frac{\omega^2}{\alpha_1^2}J_n(k_{\alpha 1}r_B), \qquad b_2 = 0, \qquad b_3 = 0,$$

$$b_4 = -\frac{i}{2}\varepsilon_n(-1)^n H_n^{(2)}(k_{\alpha 1}r_0)\left[\frac{n}{r_B}J_n(k_{\alpha 1}r_B) - k_{\alpha 1}J_{n+1}(k_{\alpha 1}r_B)\right],$$

$$b_5 = 0, \qquad b_6 = 0, \qquad b_7 = 0, \qquad b_8 = 0.$$

If the source is placed in the inner fluid, the terms b_j are defined as

$$b_1 = 0, \qquad b_2 = 0, \qquad b_3 = 0, \qquad b_4 = 0, \qquad b_5 = \frac{i}{2}\varepsilon_n(-1)^n J_n(k_{\alpha 2}r_0)\lambda_2\frac{\omega^2}{\alpha_2^2}H_n^{(2)}(k_{\alpha 2}r_A),$$

$$b_6 = 0, \qquad b_7 = 0, \qquad b_8 = -\frac{i}{2}\varepsilon_n(-1)^n J_n(k_{\alpha 2}r_0)\left[\frac{n}{r_A}H_n^{(2)}(k_{\alpha 2}r_A) - k_{\alpha 2}H_{n+1}^{(2)}(k_{\alpha 2}r_A)\right].$$

References

[1] G. Liu, J. Qu, Transient wave propagation in a circular annulus subjected to transient excitation on its outer surface, J. Acoust. Soc. Am. 104 (3) (1998) 1210–1220.

[2] J. Chung, J. Lee, Vibration analysis of a nearly axisymmetric shell structure using a new finite ring element, J. Sound Vib. 219 (1) (1999) 35–50.

[3] R. Hwang, C. Fox, S. McWilliam, The in-plane vibration of thin rings with in-plane profile variations. Part I. General background and theoretical formulation, J. Sound Vib. 220 (3) (1999) 497–516.

[4] C. Fox, R. Hwang, S. McWilliam, The in-plane vibration of thin rings with in-plane profile variations. Part II. Application to nominally circular rings, J. Sound Vib. 220 (3) (1999) 517–539.

[5] R. Hwang, C. Fox, S. McWilliam, Free vibrations of elliptical rings with circumferentially variable thickness, J. Sound Vib. 228 (3) (1999) 683–699.

[6] N. Veksler, J. Izbicki, J. Conoir, Bending a wave in the scattering by a circular cylindrical shell: its relation with the bending free modes, J. Acoust. Soc. Am. 96 (1) (1994) 287–293.

[7] X.L. Bao, P.K. Raju, H. Uberall, Circumferential waves on an immersed, fluid-filled elastic cylindrical shell, J. Acoust. Soc. Am. 105 (5) (1999) 2704–2709.

[8] G. Maze, J. Cheeke, X. Li, Z. Wang, Coupled guided acoustic modes in water-filled thin-walled tubes, J. Acoust. Soc. Am. 110 (5) (2001) 2295–2300.

[9] A. Tadeu, L. Godinho, 3D wave scattering by a fixed cylindrical inclusion submerged in a fluid medium, Eng. Anal. Bound. Elem. 23 (1999) 745–756.

[10] M. Bouchon, K. Aki, Discrete wave-number representation of seismic-source wave field, Bull. Seismol. Soc. Am. 67 (1977) 259–277.

[11] D.E. Beskos, Boundary element methods in dynamic analysis, Part II (1986–1996), Appl. Mech. Rev. 50 (1997) 149–197.

[12] R. Phinney, Theoretical calculation of the spectrum of first arrivals in layered elastic mediums, J. Geophys. Res. 70 (1965) 5107–5123.

[13] E. Kausel, J. Roesset, Frequency domain analysis of undamped systems, J. Eng. Mech. ASCE 118 (4) (1992) 721–734.

[14] K. Graff, Wave Motion in Elastic Solids, Dover, New York, 1975.